

# Gradient-based Nested Co-Design of Aerodynamic Shape and Control for Winged Robots

Daniele Affinita, Ming Xu, Benoît Gherardi, Pascal Fua

**Abstract**—Designing aerial robots for specialized tasks, from perching to payload delivery, requires tailoring their aerodynamic shape to specific mission requirements. For tasks involving wide flight envelopes, the usual sequential process of first determining the shape and then the motion planner is likely to be suboptimal due to the inherent nonlinear interactions between them. This limitation has been motivating co-design research, which involves jointly optimizing the aerodynamic shape and the motion planner. In this paper, we present a general-purpose, gradient-based, nested co-design framework where the motion planner solves an optimal control problem and the aerodynamic forces used in the dynamics model are determined by a neural surrogate model. This enables us to model complex subsonic flow conditions encountered in aerial robotics and to overcome the limited applicability of existing co-design methods. These limitations stem from the simplifying assumptions they require for computational tractability to either the planner or the aerodynamics. We validate our method on two complex dynamic tasks for fixed-wing gliders: perching and a short landing. Our optimized designs improve task performance compared to an evolutionary baseline in a fraction of the computation time.

## I. INTRODUCTION

Aerial robots are becoming increasingly reliable and are now deployed in a broad range of real-world applications, including infrastructure inspection [1], environmental monitoring [2], and autonomous delivery [3]. Each application may have different design requirements, informed by both the dynamic maneuvers to be performed during missions, as well as the environmental conditions, such as ambient wind.

Designing aerodynamic shapes for task-specific aerial robots [4], [5] requires a skilled engineer to carefully optimize a design for each application, based on multiple complex criteria [6]. This usually involves a lengthy and iterative process of trial-and-error, comprised of manual design and experimental validation [7]. Moreover, when designing a shape as part of an autonomous system, the generally nonlinear interactions between the shape and the motion planning algorithms that are applied during autonomous operation should be considered during the design process. This requirement motivates the *algorithmic co-design* problem, which involves jointly optimizing the aerodynamic shape and motion planner to achieve improved system-level performance [8]. Co-design stands in contrast to the standard sequential design pipeline [9], [10] where the shape is designed first and the motion planner next, which has been shown to be sub-optimal [11]. An outstanding challenge for current co-design

methods is around the efficient exploration of continuous, high-dimensional design spaces that are characteristic of real design problems [12]. In particular, exhaustive exploration using sampling-based algorithms [13], [14] can become computationally intractable.

In this paper, we present a general, scalable aerodynamic co-design framework based on bilevel optimization and learned surrogate models. We jointly optimize an aerodynamic shape, here a wing profile, and a collection of optimally planned trajectories, which are the solutions to nonlinear trajectory optimization problems encoding one or more dynamic tasks [15]. Our approach falls under the *nested co-design* class of methods [16] by virtue of its bilevel formulation, meaning that optimal trajectories are found for each candidate design as the process iterates.

To make the problem tractable and to maintain adequate scaling with co-design problem complexity, we introduce several innovative mechanisms:

- 1) We use a first-order Augmented Lagrangian algorithm to solve the upper-level optimization problem, which scales linearly with the number of design parameters,
- 2) We implement an efficient differentiable optimal control for linear scaling with the planning horizon of the motion planner, as in [17].
- 3) We rely on neural surrogate models [18] to evaluate aerodynamic forces and provide a fast and differentiable alternative to computational fluid dynamics solvers. Importantly, we found it is necessary to constrain the confidence of the surrogate model predictions at the upper-level problem to prevent shapes where the surrogate model yields erroneous predictions.

We validate our framework by designing shapes for two complex dynamic maneuvers for robotic gliders, namely, a fixed-wing perching task [19] and a minimum-distance landing task. This requires handling challenging sub-sonic flow regime with significant boundary layer effects. In other words, our algorithm can optimize aerodynamic shapes in significantly wider flight envelopes, including post-stall, than earlier aerodynamic co-design works focusing on hypersonic vehicles [20], [21]. Thus, it opens up numerous potential applications of nested co-design more generally, including but not limited to aerial robotics.

## II. RELATED WORK

The co-design of plants and controllers have been studied for motorcycles [22], network-controlled systems [23], and floating offshore wind turbines [24], in addition to aerospace and robotics. For a broader overview of co-design in other

All authors are with École Polytechnique Fédérale de Lausanne (EPFL), Lausanne, Switzerland {daniele.affinita, mingda.xu, benoit.gherardi, pascal.fua}@epfl.ch

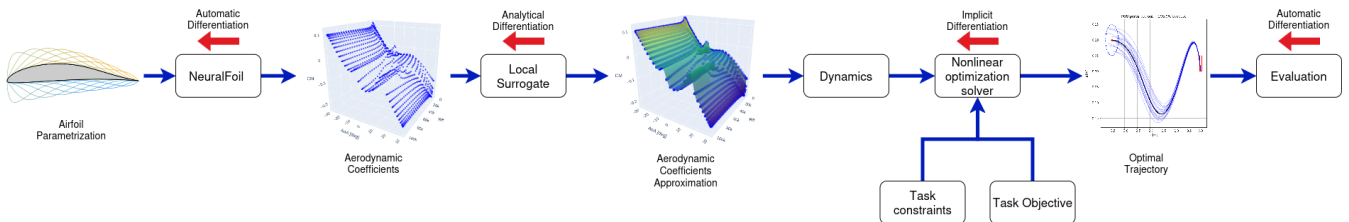


Fig. 1: Overview of the proposed co-design pipeline. The airfoil parameterization is mapped to aerodynamic coefficients by a differentiable neural surrogate, from which a local surrogate is built and embedded in the system dynamics. A nonlinear trajectory optimization problem, defined by task objectives and constraints, is then solved and the resulting optimal trajectories evaluated. Gradients are propagated through the solver via implicit differentiation, and through the remaining components via analytical and automatic differentiation, enabling end-to-end optimization.

domains, see [25]. For brevity, we limit ourselves to the last two here.

*a) Robotics:* In robotics, co-design is commonly formulated over discrete component choices (e.g., motors, sensors, and actuators) or low-dimensional continuous parameterizations. Thus, it rarely tackles direct optimization of continuous airfoil geometries in high-dimensional design spaces, where Bayesian optimization becomes sample-inefficient [26]. Evolutionary algorithms can optimize design and control parameters [27], [14], but require many expensive simulations and scale poorly with dimensionality [28]. This is precisely the challenge we address.

For discrete co-design, [7] formulates the problem as a binary linear program to maximize task performance, which is efficient in discrete spaces but unsuitable for geometric design with continuous parameters. Hybrid discrete–continuous methods [13] optimize topology and continuous variables, yet typically neglect nonlinear aerodynamics and rely on linearized dynamics, limiting them to simple tasks such as straight-line flight. In contrast, we address continuous geometric co-design with nonlinear aerodynamics.

*b) Aerospace:* In aerospace, unlike robotics, co-design methods often leverage gradient-based nested optimization to handle high-dimensional continuous design spaces, with accurate aerodynamic models. A framework for controlled aerodynamic co-design was proposed in [21], optimizing a supersonic missile using computational fluid dynamics (CFD) and continuous adjoint methods [29]. However, their linear policy limits expressiveness, and using finite differences for sensitivities reduces scalability. In contrast, our approach optimizes over time-varying control trajectories and computes exact sensitivities through the optimal control problem, enabling more complex maneuvers to be co-designed with the geometry.

Our approach is in the same spirit as that of [20] that extends co-design to hypersonic glide vehicles using a gradient-based bilevel pipeline. This method scales well with the number of design parameters and eliminates the need for finite differences. However, the flight envelope is restricted to reduce the number of CFD evaluations and relies on inviscid flow assumptions, limiting applicability to the hypersonic regime and neglecting viscous and separated flow effects. In contrast, we employ a neural network surrogate to capture

aerodynamic effects without restricting the operating regime.

### III. METHODOLOGY

In this section, we introduce the formulation of the aerodynamic co-design problem and describe the proposed framework. For brevity and concreteness, we introduce our co-design framework using a specific example that we use for evaluation in Section IV, namely, planar unpowered flight. However, the methodology is not restricted to this setting and applies to more general dynamical systems. Fig. 1 illustrates the structure of the approach.

#### A. Problem Formulation

Let  $\psi \in \mathbb{R}^d$  denote the design parameters of the robot shape. Let  $x_t$  be the system state at discrete time step  $t$  and  $u_t$  the control input. For a given design  $\psi$ , the finite-horizon optimal control problem (OCP) returns the optimal trajectories  $x_{1:N}^*(\psi)$  and  $u_{1:N-1}^*(\psi)$ . Our nested aerodynamic co-design problem can then be defined as

$$\begin{aligned} \min_{\psi} \quad & \Phi(\psi, x_{1:N}^*(\psi), u_{1:N-1}^*(\psi)) \\ \text{subject to} \quad & h(\psi) = 0 \\ & g(\psi) \leq 0 \end{aligned} \quad (1)$$

where  $h(\cdot)$  and  $g(\cdot)$  denote the equality and inequality constraints of the upper problem, respectively. These constraints typically encode geometric or structural requirements on the design, preventing degenerate or impossible to manufacture solutions. The upper objective  $\Phi(\cdot)$  can represent the total cost over one or more trajectory tasks represented by OCPs, each corresponding to different flight conditions, objectives, or initial states. In this multi-task setting, the costs or constraint violations from all trajectories are aggregated (e.g., by averaging) to yield a single design  $\psi^*$  that performs robustly across all considered scenarios.

The optimal trajectories  $x_{1:N}^*(\psi)$  and  $u_{1:N-1}^*(\psi)$  are defined implicitly as the solution to the OCP

$$\begin{aligned} \min_{x_{1:N}, u_{1:N-1}} \quad & \sum_{t=0}^N \ell(x_t, u_t) + \ell_f(x_N) \\ \text{subject to} \quad & x_1 = \hat{x}_1 \\ & c(x_t, u_t) = 0 \quad \text{for } t \in [N] \\ & d(x_t, u_t) \leq 0 \quad \text{for } t \in [N] \\ & x_{t+1} = f(x_t, u_t; \psi) \quad \text{for } t \in [N-1], \end{aligned} \quad (2)$$

where,  $\hat{x}_1$  is the initial state,  $\ell(\cdot)$  the stage cost,  $\ell_f(\cdot)$  the terminal cost, and  $c(\cdot)$  and  $d(\cdot)$  the equality and inequality constraints along the trajectory. The system dynamics  $x_{t+1} = f(x_t, u_t; \psi)$  depend on the design parameters, capturing how variations in geometry affect the aerodynamics.

### B. Flight Dynamics Model

For our 3-DoF unpowered flight example, the system state is defined as

$$\mathbf{x} = [x \ z \ \theta \ \phi \ \dot{x} \ \dot{z} \ \dot{\theta}]^\top \quad (3)$$

where  $(x, z)$  is the center-of-mass position,  $\theta$  the pitch angle,  $\phi$  the elevator angle relative to the fuselage, and  $(\dot{x}, \dot{z}, \dot{\theta})$  the translational and angular velocities. The control input is the elevator angular velocity  $u = \dot{\phi}$ .

We adopt the planar rigid-body dynamics model [19] for gliders, where the robot is modeled as a rigid body comprised of three parts: the fuselage, wings, and elevator. Aerodynamic forces are assumed to only act on the two lifting surfaces. For brevity, only wing forces are detailed; analogous expressions hold for the elevator.

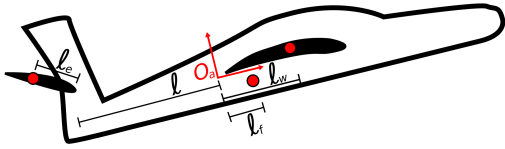


Fig. 2: Glider schematic. The red dots indicate the centers of mass of the fuselage, wing, and elevator. The notation is described in Tab. II

In contrast to [19], where the aerodynamic coefficients are computed using a flat-plate assumption, we employ an aerodynamic surrogate model  $\mathcal{N}(\psi)$ , which we describe in detail in Sec. III-C. The model defines a mapping

$$\mathcal{N}_\zeta : (\psi, \alpha, Re) \mapsto (C_L, C_D, C_M) \quad (4)$$

where  $C_L$ ,  $C_D$ , and  $C_M$  are the lift, drag, and moment coefficients, respectively,  $\alpha$  and  $Re$  are the angle of attack and Reynolds number of the lifting surface, both determined by the robot's kinematics and  $\zeta$  are model parameters.

The magnitude of aerodynamic forces and moment acting on the wing, namely the lift  $F_w^L$ , drag  $F_w^D$ , and pitching moment  $M_w$ , are given by:

$$\begin{aligned} F_w^L &= \frac{1}{2} \rho \|\mathbf{v}_w\|^2 S_w C_L(\alpha_w, Re_w, \psi) \\ F_w^D &= \frac{1}{2} \rho \|\mathbf{v}_w\|^2 S_w C_D(\alpha_w, Re_w, \psi) \\ M_w &= \frac{1}{2} \rho \|\mathbf{v}_w\|^2 S_w \bar{c}_w C_M(\alpha_w, Re_w, \psi) \end{aligned} \quad (5)$$

where  $S_w$  is the wing surface area,  $\rho$  the air density,  $\mathbf{v}_w$  the velocity of the airflow relative to the wing,  $\bar{c}_w$  the wing mean chord. The final force acting on the wing is defined as

$$\mathbf{F}_w = -F_w^D \mathbf{n}_w + F_w^L \mathbf{n}_{w\perp} \quad (6)$$

where  $\mathbf{n}_w = \mathbf{v}_w / \|\mathbf{v}_w\|$  and  $\mathbf{n}_{w\perp}$  is perpendicular to  $\mathbf{n}_w$ , oriented upward (coinciding with the positive  $z$  direction when  $\theta = 0$ ).

Finally, the dynamics are given by the rigid-body equations for the glider:

$$\begin{aligned} \begin{bmatrix} m\ddot{x} \\ m\ddot{z} \end{bmatrix} &= \mathbf{F}_w + \mathbf{F}_e + \begin{bmatrix} 0 \\ -mg \end{bmatrix} \\ I\ddot{\theta} &= \mathbf{r}_w \times \mathbf{F}_w + \mathbf{r}_e \times \mathbf{F}_e + M_w + M_e \end{aligned} \quad (7)$$

where  $\mathbf{r}_w$  and  $\mathbf{r}_e$  denote the vectors from the center of mass to the aerodynamic centers of the wing and elevator, respectively. Here,  $g$  is the gravitational acceleration.

### C. Aerodynamic Surrogate Models

The aerodynamic coefficients are provided by the surrogate model NeuralFoil [18], a physics-informed deep neural network trained on a large corpus of high-fidelity simulations and wind-tunnel data. It is well-suited to our problem since small fixed-wing aerial robots operate at lower speeds and perform more aggressive trajectories than conventional aircraft, resulting in lower Reynolds numbers and excursions to extreme angles of attack that fall outside the validity range of tools designed for traditional aviation. NeuralFoil is designed to remain robust over the full  $360^\circ$  angle-of-attack range and for Reynolds numbers spanning  $10^2$  to  $10^{10}$ , whereas traditional solvers such as XFOIL [30] frequently fail to converge in these conditions.

From a computational and optimization standpoint, the surrogate model enables scalability gains. NeuralFoil achieves a speedup of approximately  $1000\times$  over XFOIL at a comparable accuracy level [18], reducing the evaluation time from seconds to milliseconds per query. Moreover, XFOIL does not guarantee  $C^1$  continuity of the aerodynamic coefficients with respect to its inputs, whereas NeuralFoil is  $C^\infty$  almost everywhere. This smoothness, together with its full differentiability, enables gradient-based optimization within the proposed bilevel co-design framework. Being partially trained on XFOIL data, NeuralFoil retains the accuracy of well-converged traditional solutions while delivering consistent and numerically robust predictions in challenging flow regimes. The model also outputs a confidence value for each prediction; when this value is too low, the predicted coefficients are considered unreliable.

a) *Confidence Constraint*: To ensure reliable predictions from the NeuralFoil surrogate, we require a minimum confidence of our predictions within the upper problem of Eq. (1). Thus, we enforce

$$c(\psi, \alpha, Re) \geq c_{\min} \quad \forall (\alpha, Re) \in \mathcal{E}, \quad (8)$$

where  $c(\psi, \alpha, Re)$  is the confidence output by NeuralFoil for a given airfoil design  $\psi$  and flow conditions  $(\alpha, Re)$ . The confidence output reflects how closely the queried airfoil geometry lies to the training distribution of the surrogate; low-confidence regions correspond to out-of-distribution airfoil shapes where the model's predictions are no longer faithful. Without this constraint, the optimizer can take

advantage of regions with low confidence. This may lead to physically unrealistic designs, such as excessively thin or highly undulating airfoil shapes, which produce unphysical forces and moments. Enforcing  $c \geq c_{\min}$  prevents such degenerate shapes, ensuring that the surrogate is evaluated only in regions of the design space where it is reliable. The confidence threshold  $c_{\min}$  is chosen empirically to balance feasibility and design flexibility.

*b) Motivation for a Local Approximation:* The aerodynamic coefficients ( $C_L, C_D, C_M$ ) and their derivatives (up to second order with respect to  $(\alpha, Re)$ ) are evaluated at every iteration of the inner OCP solver for each timestep in the planning horizon. The cost of each evaluation is  $O(|\zeta|)$ , where  $\zeta$  are the network parameters. As a concrete example, NeuralFoil’s XXL variant has over 1 million parameters, rendering this computation a huge bottleneck for the algorithm. To address this, we introduce a local polynomial surrogate of NeuralFoil solved for a fixed shape  $\psi$ . This polynomial with parameters  $w$  of order hundreds, provides a smooth and differentiable approximation to the underlying neural surrogate, with  $O(|w|)$  complexity with  $|w| \ll |\zeta|$ .

*c) Chebyshev Polynomial Approximation:* For a fixed design  $\psi$ , NeuralFoil is approximated over a prescribed flight envelope  $\mathcal{E} = \{(\alpha, Re)\}$  using a bivariate Chebyshev polynomial [31] of degree  $k$ . The polynomial is fit using samples  $\{(\alpha_i, Re_i)\}_{i=1}^M \subset \mathcal{E}$  determined using the Chebyshev node strategy [32], which mitigates boundary oscillations and the Runge phenomenon. Let  $\varphi(\alpha, Re) \in \mathbb{R}^{k^2}$  denote the vector of values of the Chebyshev basis evaluated at  $\alpha, Re$ . The aerodynamic coefficients are then approximated as

$$(C_L, C_D, C_M) \approx \varphi(\alpha, Re)^\top w,$$

where  $w$  contains the polynomial coefficients.

The coefficient vector  $w$  is obtained by solving a least-squares problem over a set of sampled flight conditions introduced above, formally defined as

$$w^*(\psi) = \arg \min_w \sum_{i=1}^M \|\varphi(\alpha_i, Re_i)^\top w - \mathcal{N}(\psi, \alpha_i, Re_i)\|^2.$$

#### D. Algorithm

The upper problem Eq. (1) is solved using a gradient-descent method applied to the *Augmented Lagrangian* [33]

$$\begin{aligned} \mathcal{L}(\psi, \lambda, \nu, \mu) = & \Phi(\psi) + \lambda^\top h(\psi) + \frac{\mu}{2} \|h(\psi)\|^2 \\ & + \nu^\top \max(0, g(\psi)) + \frac{\mu}{2} \|\max(0, g(\psi))\|^2, \end{aligned} \quad (9)$$

which enforces the equality and inequality constraints of Eq. (1). The Lagrange multipliers  $\lambda$  and  $\nu$  are updated at each iteration proportional to the current constraint violation to enforce satisfaction more strictly. To apply gradient descent, we need the gradient of the augmented Lagrangian with respect to the design parameters  $\psi$ , which requires the full pipeline, including the inner OCP, to be differentiable. This will be described in the remainder of this section.

For motion planning, the inner OCP is solved using a nonlinear optimization method, with constraints that include

the system dynamics. The aerodynamic coefficients in these dynamics are approximated using the bivariate Chebyshev polynomial surrogate introduced in Sec. III-C.

*a) Efficient sensitivities:* To embed the inner OCP Eq. (2) in the bilevel problem Eq. (1) and solve it using gradient-based optimization, we require sensitivities of the OCP solution with respect to polynomial coefficients  $w$ . Naively, computing these sensitivities would involve solving the full set of KKT conditions as a dense system, resulting in cubic complexity in the horizon length,  $O(N^3)$  [17]. We overcome this by computing the sensitivities via implicit differentiation using the structure-exploiting approach of [17], which leverages the block-sparse structure of the dynamics. This yields the sensitivities  $D_w x_{1:N}^*$  and  $D_w u_{1:N-1}^*$  with linear complexity,  $O(N)$ , in the horizon length. Derivatives of the polynomial coefficients with respect to the design parameters,  $D_\psi w^*$ , as well as the evaluation of upper objectives and constraints, are computed via Automatic Differentiation. All contributions are then combined through the chain rule to obtain the gradient of the upper problem,  $\nabla_\psi \mathcal{L}$ , enabling efficient and scalable gradient-based optimization of the bilevel problem.

## IV. EXPERIMENTAL EVALUATION

We validate our co-design framework on two challenging tasks for gliders: perching at a precise location as first proposed in [19] and minimum distance landing, described in more detail below. We compare our results against three baselines described in Sec. IV-B.

### A. Perching and Landing Tasks

We now describe our two tasks in more detail.

*a) Perching:* Perching requires the robot to reach a fixed location with near-zero velocity, mimicking the way a bird would land on a wire. We set the initial dynamic state of the robot with a position far back from the perch, such that the perching task is not achievable with the initial design.

*b) Minimum Distance Landing:* The minimum distance landing task requires the robot to land softly on the ground while trying to minimize the horizontal distance traveled.

Both tasks are defined as OCPs of form Eq. (2). The system state  $\mathbf{x}$  is defined in Eq. (3), the control input  $u$  corresponds to the elevator angular velocity. We also include the time step discretization  $h$  as an additional decision variable, following the formulation of perching from [19]. Both tasks can be formulated using cost functions of form

$$\begin{aligned} \ell(x_t, u_t, h_t) = & h_t \left( \|x_t - x_{\text{target}}\|_Q^2 + R u_t^2 \right) + S h_t^2, \\ \ell_f(x_N) = & \|x_N - x_{\text{target}}\|_Q^2, \end{aligned} \quad (10)$$

where  $Q \succeq 0$ ,  $R \geq 0$ , and  $S \geq 0$ . The perching and minimum distance landing task uses different parameters in the OCP formulation. We list the parameters of the OCP in Tab. I. In addition to the system dynamics and initial state, the OCP enforces the actuator constraint on the elevator

$$-\pi/3 \leq \phi_t \leq \pi/8, \quad |\dot{\phi}_t| \leq 13 \quad \text{for } t \in [N] \quad (11)$$

Tab. I summarizes the task-specific parameters of the inner optimal control problem. For both tasks, we use a control effort weight  $R = 0.001$  and a time penalty weight  $S = 0.01$ .

### B. Comparison Methods

We compare our gradient-based co-design framework against three baselines that represent standard design and co-design strategies:

- 1) *Fixed*. Using a reference NACA 4412 airfoil without modifications, serving as a lower bound on what is achievable without aerodynamic optimization.
- 2) *Sequential*. A traditional sequential pipeline commonly used in industry [34], where the airfoil is first optimized using a proxy metric, and the control strategy is designed next with a fixed airfoil shape. For the perching task, the proxy is the lift-to-drag ratio: since the glider starts far from the perch, maximizing glide efficiency is a natural surrogate for reaching the target accurately. For minimum-distance landing, the drag coefficient is maximized subject to a minimum lift-to-drag constraint to enable rapid slowing required for the manoeuvre. Both tasks involve post-stall and high angle-of-attack flight phases of varying length, making the choice of proxy metric inherently difficult to justify.
- 3) *Evolutionary*. A state-of-the-art evolutionary co-design strategy [14] which jointly optimizes the airfoil geometry and control policy using an evolutionary algorithm. Evolutionary algorithms maintain a population of candidate solutions that evolve across generations through selection, crossover, and mutation, exploring the design space without requiring gradient information. Unlike the sequential approach, this baseline accounts for the coupling between design and control. The evolutionary process is implemented using *Deap* library [35], and it is characterized by a population of 50 individuals, single-point crossover ( $p=90\%$ ), random mutation ( $p=6\%$ ), and a stop criterion after 100 generations.

### C. Co-Design Objective

The aerodynamic design is parameterized using the Kulfan universal representation [36], which expresses the upper and lower surfaces as linear combinations of class and shape functions weighted by design parameters  $\psi \in \mathbb{R}^{18}$ . Our co-design objective optimizes these parameters to improve overall flight performance.

To assess robustness to variations in the initial state, we solve multiple OCP instances in parallel for each aerodynamic design, corresponding to different starting positions and velocities. By evaluating performance across this ensemble of initial conditions, the optimization encourages designs that perform well over a broader range of scenarios, rather than being tailored to a single starting state. Let  $\{x_N^{*(i)}\}_{i=1}^K$  denote the terminal states of the optimal  $K$  trajectories. We define the co-design objective as

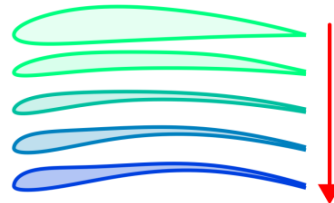
$$\Phi(\psi) = \frac{1}{K} \sum_{i=1}^K \ell_f(x_N^{*(i)}(\psi)), \quad (12)$$

We set the minimum confidence threshold for NeuralFoil predictions to  $c_{min} = 0.6$  in Eq. (8). Additionally, we introduce a minimum lift-to-drag ratio constraint

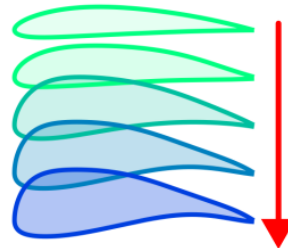
$$\frac{C_L(\psi, \alpha, Re)}{C_D(\psi, \alpha, Re)} \geq 2.5 \quad \forall(\alpha, Re) \in \mathcal{E} \quad (13)$$

to ensure that the optimal design satisfies global aerodynamic performance requirements and that the resulting airfoil can also operate efficiently in normal cruise conditions.

Finally, a minimum airfoil thickness of 5% of the chord is enforced across all chord-wise locations in the Kulfan parameter space to ensure structural integrity and manufacturability.



(a) Perching task: airfoil becomes thinner and more cambered.



(b) Landing task: leading edge thickens to increase drag while the trailing edge remains slender for controllability.

Fig. 3: Airfoil shape evolution across iterations for the perching (a) and landing (b) tasks. The geometries progressively adapt to the aerodynamic requirements of each task.

### D. Experimental Setup

The upper optimization is performed using the Adam optimizer for the airfoil parameters, and the inner OCP is solved using IPOPT [37], a primal-dual interior-point method. We run 80 upper iterations using an initial learning rate of 0.01 and an exponential decay schedule with  $\gamma = 0.99$ . The Augmented Lagrangian Eq. (9) initial penalty parameter is set to  $\mu = 10$ , and for all experiments, the airfoil shape is initialized from the NACA 4412 airfoil.

### E. Platform

Fig. 2 illustrates the system geometric parameters, while Tab. II lists the numerical values used in the experiments.

		$x$	$z$	$\theta$	$\phi$	$\dot{x}$	$\dot{z}$	$\dot{\theta}$
Perching	$x_{target}$	0	0	0	0	0	0	0
	$Q$	10	10	5	0.01	5	5	2
	Initial State 1	-8.5	1	0	0	6	3	0
	Initial State 2	-8.5	0	0	0	6	3	0
	Initial State 3	-10	1	0	0	6	3	0
Initial State 4	-10	0	0	0	6	3	0	
Landing	$x_{target}$	0	0	0	0	0	0	0
	$Q$	5	50	2	0	0	5	0
	Initial State 1	0	2	0	0	6	0	0
	Initial State 2	0	3	0	0	6	0	0
	Initial State 3	0	4	0	0	6	0	0
Initial State 4	0	5	0	0	6	0	0	

TABLE I: Target states, penalty weights ( $Q$ ), and initial conditions for Perching and Landing tasks.

$m_f$	$m_w$	$m_e$	$\ell$	$\ell_e$	$\ell_f$	$\ell_w$	$S_w$	$S_e$
0.026	0.035	0.004	0.260	0.020	-0.027	-0.010	0.158	0.017

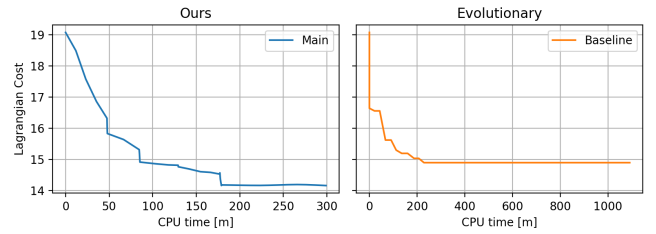
TABLE II: Glider parameters used in the experiments.  $\ell$  denotes lengths from the glider origin ( $m$ ),  $m$  masses ( $kg$ ), and  $S$  surface areas ( $m^2$ ). Subscripts indicate the corresponding body:  $w$  wing,  $e$  elevator,  $f$  fuselage.

## F. Results

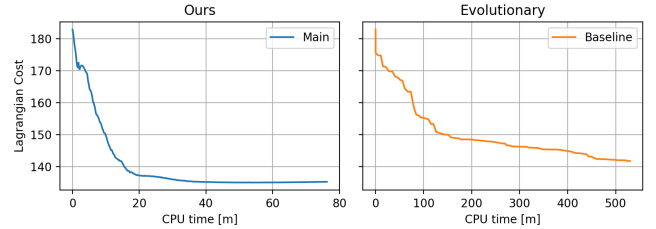
Our experimental results are reported in Tab. III. Across both tasks, the proposed gradient-based co-design pipeline consistently outperforms all baselines presented in IV-B, while converging in a fraction of the computation time as shown in Figs. 4a and 4b.

*a) Computational efficiency:* Beyond solution quality, a key practical advantage of the proposed approach is its efficiency. The perching optimization converges in approximately 3 hours, and the landing optimization in under 1 hour, both on a consumer-grade laptop equipped with an Intel Core i9-14900HX CPU and an NVIDIA GeForce RTX 4060 GPU. By contrast, the genetic algorithm of [14] was allocated 24 hours for the perching task and 12 hours for the landing task, yet still achieved worse results. This order of magnitude reduction validates our claim that gradient-based co-design scales efficiently to continuous, high-dimensional airfoil design spaces, where population-based search becomes computationally intractable. Figs. 4a and 4b show the evolution of the Lagrangian cost, illustrating the faster convergence of our framework compared to the genetic algorithm.

*b) Perching Task:* Fig. 3a illustrates how the airfoil geometry evolves over the course of the perching optimization, and Fig. 6b shows the corresponding trajectories. The optimizer drives the geometry toward a thinner, more cambered profile. This shape improves aerodynamic efficiency and controllability, enabling the glider to reach the perch with higher positional accuracy and lower terminal velocity. While this trend is physically intuitive, it is important to note that it emerges entirely from the task objective rather than from any aerodynamic proxy. This distinction is underscored by the sequential baseline results. It explicitly optimizes the lift-to-drag ratio and yet performs worse on the perching task, highlighting that task-agnostic aerodynamic heuristics



(a) Perching task.



(b) Landing task.

Fig. 4: Comparison of the Lagrangian cost between our framework and the evolutionary algorithm [14] for the perching (a) and landing (b) tasks. For the evolutionary algorithm, the best fitness value found across all individuals in the current and all previous generations is plotted. The x-axis shows CPU time in minutes.

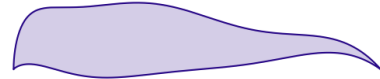
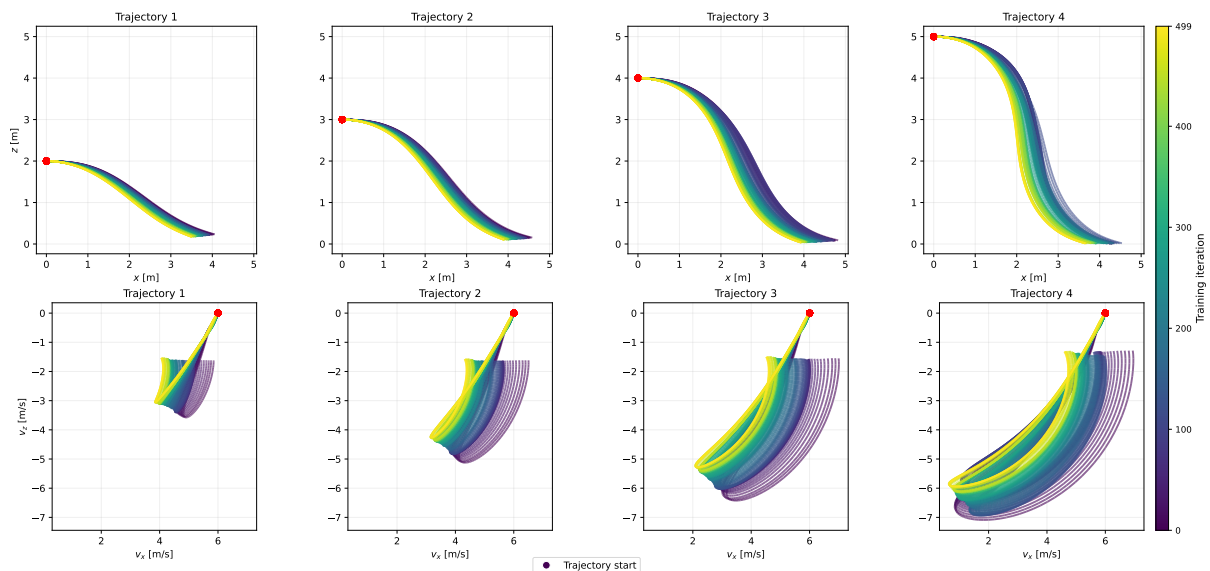


Fig. 5: Degenerate airfoil obtained by optimizing lift-to-drag ratio without the NeuralFoil confidence constraint. The geometry collapses to an aphysical shape with near-zero surrogate confidence.

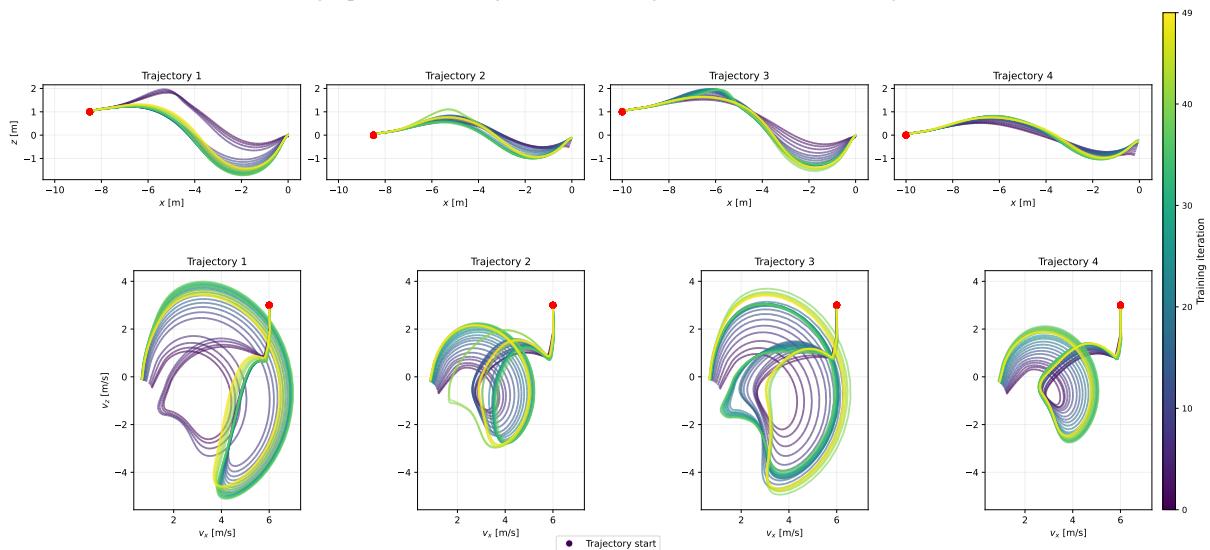
are suboptimal surrogates for mission performance.

*c) Minimum Distance Landing Task:* It reveals a qualitatively different but equally interpretable optimization behavior. As shown in Figs. 3b and 6a, the optimizer produces a geometry with a thicker leading region and a thinner trailing section. The thick leading edge increases drag, dissipating energy rapidly and shortening the landing distance, while the tapered tail preserves a minimum level of aerodynamic efficiency to maintain controlled flight throughout the approach. Once again, the sequential design baseline fails to match this performance: maximizing drag subject to a minimum lift-to-drag constraint is an imperfect proxy for the actual landing cost, and the gap in Tab. III reflects this.

*d) Importance of the Confidence Constraint:* A critical component of the pipeline is the NeuralFoil confidence constraint, which prevents the optimizer from exploiting regions of the surrogate model where aerodynamic predictions are no longer physically meaningful. Fig. 5 illustrates what happens when this constraint is removed: the optimizer converges to an implausible geometry with a seemingly very high lift-to-drag ratio but an average NeuralFoil confidence near zero, meaning the aerodynamic force predictions are



(a) Landing optimization: trajectories converge toward shorter landing distances.



(b) Perching optimization: trajectories converge toward lower terminal velocities and tighter positional accuracy at the perch.

Fig. 6: Evolution of state trajectories (top) and velocity profiles (bottom) for the landing (a) and perching (b) optimizations. Each plot shows results from four initial conditions, with darker lines for earlier iterations and lighter lines for later ones.

Method	Perching OCP ↓	Landing OCP ↓
Fixed	19.06	182.94
Sequential	15.60	220.35
Evolutionary [14]	14.91	139.73
<b>Ours</b>	<b>13.43</b>	<b>131.01</b>

↓ lower is better

TABLE III: OCP cost comparison across methods for the perching and landing tasks under identical constraints.

entirely unreliable. This result confirms that without explicit regularization of the surrogate’s validity domain, gradient-based optimization will find and exploit model artifacts rather than aerodynamic improvements.

## V. CONCLUSION

In this paper, we presented a scalable bilevel co-design framework that jointly optimizes aerodynamic shape and motion planning. By combining a gradient-based Augmented Lagrangian upper optimizer with differentiable optimal control and a learned aerodynamic surrogate, our approach optimizes continuous, high-dimensional design spaces that are intractable for sampling-based methods. A key finding is that constraining the surrogate’s confidence is essential to prevent gradient-based optimization from exploiting out-of-distribution regions of the model. Although the presented approach is general and can be applied across multiple domains, we validate it on a propeller-less aerial robot performing two challenging trajectories: perching and minimum

distance landing. Our experiments demonstrate that the proposed framework consistently outperforms fixed, sequential, and evolutionary baselines on both tasks, while converging in a fraction of the computation time.

*a) Future Work:* While the current work focuses on 2D aerodynamic design and planar trajectories, the framework is completely general and designed to scale to more complex problems. A natural and immediate extension is to 3D airfoil design coupled with full 3D aerobatic trajectory optimization, enabling richer trajectories that go well beyond the planar setting considered here. More broadly, the bilevel structure of our pipeline is compatible with mixed-integer optimization, which would allow the framework to jointly optimize both individual component shapes and the overall system topology, opening the door to automated structural design of aerial robots.

## REFERENCES

- [1] A. J. Lee, W. Song, B. Yu, D. Choi, C. Tirtawardhana, and H. Myung, "Survey of robotics technologies for civil infrastructure inspection," *Journal of Infrastructure Intelligence and Resilience*, 2023.
- [2] N. H. Motlagh, P. Kortoçi, X. Su, L. Lovén, H. K. Hoel, S. B. Haugsvær, V. Srivastava, C. F. Gulbrandsen, P. Nurmi, and S. Tarkoma, "Unmanned aerial vehicles for air pollution monitoring: A survey," *IEEE Internet of Things Journal*, 2023.
- [3] J. Grzybowski, K. Latos, and R. Czyba, "Low-cost autonomous uav-based solutions to package delivery logistics," in *Advanced, Contemporary Control: Proceedings of KKA 2020—The 20th Polish Control Conference, Łódź, Poland, 2020*. Springer, 2020.
- [4] H. Karali, G. Inalhan, and A. Tsourdos, "Advanced uav design optimization through deep learning-based surrogate models," *Aerospace*, 2024. [Online]. Available: <https://www.mdpi.com/2226-4310/11/8/669>
- [5] A. Papageorgiou, M. Tarkian, K. Amadori, and J. Ölvander, "Multidisciplinary design optimization of aerial vehicles: A review of recent advancements," *International Journal of Aerospace Engineering*, 2018.
- [6] A. Sobester and A. Keane, "Multidisciplinary design optimization of uav airframes," in *47th AIAA/ASME/ASCE/AHS/ASC Structures, Structural Dynamics, and Materials Conference; 14th AIAA/ASME/AHS Adaptive Structures Conference*, 2006.
- [7] L. Carlone and C. Pinciroli, "Robot co-design: beyond the monotone case," in *2019 International Conference on Robotics and Automation (ICRA)*. IEEE, 2019.
- [8] J. T. Allison and S. Nazari, "Combined plant and controller design using decomposition-based design optimization and the minimum principle," in *International design engineering technical conferences and computers and information in engineering conference*, 2010.
- [9] D. Raymer, *Aircraft design: a conceptual approach*. American Institute of Aeronautics and Astronautics, Inc., 2012.
- [10] J. R. Martins and A. B. Lambe, "Multidisciplinary design optimization: a survey of architectures," *AIAA journal*, 2013.
- [11] E. Fernández Bravo, M. Ornik, and J. T. Allison, "Numerical Estimation of Bidirectional Plant-Control Design Coupling in Control Co-Design," in *International Design Engineering Technical Conferences and Computers and Information in Engineering Conference*, vol. 88360, 2024.
- [12] D. A. Masters, N. J. Taylor, T. Rendall, C. B. Allen, and D. J. Poole, "Geometric comparison of aerofoil shape parameterization methods," *AIAA journal*, 2017.
- [13] A. Zhao, T. Du, J. Xu, J. Hughes, J. Salazar, P. Ma, W. Wang, D. Rus, and W. Matusik, "Automatic co-design of aerial robots using a graph grammar," in *2022 IEEE/RSJ International Conference on Intelligent Robots and Systems (IROS)*, 2022.
- [14] F. Bergonti, G. Nava, V. Wüest, A. Paolino, G. L'Erario, D. Pucci, and D. Floreano, "Co-design optimisation of morphing topology and control of winged drones," in *2024 IEEE International Conference on Robotics and Automation (ICRA)*. IEEE, 2024. [Online]. Available: <http://dx.doi.org/10.1109/ICRA57147.2024.10611506>
- [15] M. Kelly, "An introduction to trajectory optimization: How to do your own direct collocation," *SIAM review*, 2017.
- [16] J. Wauters, T. Lefebvre, and G. Crevecoeur, "Comparative study of co-design strategies for mission-specific design of quadcopters using differential flatness and bayesian optimization," in *2022 IEEE/ASME International Conference on Advanced Intelligent Mechatronics (AIM)*, 2022.
- [17] M. Xu, T. L. Molloy, and S. Gould, "Revisiting implicit differentiation for learning problems in optimal control," *Advances in Neural Information Processing Systems*, 2023.
- [18] P. Sharpe and R. J. Hansman, "Neuralfoil: An airfoil aerodynamics analysis tool using physics-informed machine learning," *arXiv preprint arXiv:2503.16323*, 2025.
- [19] J. Moore, R. Cory, and R. Tedrake, "Robust post-stall perching with a simple fixed-wing glider using lqr-trees," *Bioinspiration & biomimetics*, 2014.
- [20] K. Mackle, A. Lock, I. Jahn, and C. van der Heide, "Developing a co-design framework for hypersonic vehicle aerodynamics and trajectory," in *AIAA SCITECH 2024 Forum*, 2024.
- [21] K. W. Lee, W. Moase, A. Ooi, C. Manzie, and E. C. Kerrigan, "Optimization framework for codesign of controlled aerodynamic systems," *AIAA Journal*, 2016.
- [22] S. Evangelou, D. J. Limebeer, R. S. Sharp, and M. C. Smith, "Control of motorcycle steering instabilities," *IEEE Control Systems Magazine*, 2006.
- [23] M. S. Branicky, S. M. Phillips, and W. Zhang, "Scheduling and feedback co-design for networked control systems," in *Proceedings of the 41st IEEE Conference on Decision and Control*, 2002. IEEE, 2002.
- [24] L. Y. Pao, M. Pusch, and D. S. Zalkind, "Control co-design of wind turbines," *Annual Review of Control, Robotics, and Autonomous Systems*, 2024.
- [25] J. G. d. Silva, T. Nazaré, M. Costa, M. J. Lacerda, and E. Nepomuceno, "Engineering and technology applications of control co-design: A survey," *IEEE Access*, 2024.
- [26] M. Malu, G. Dasarathy, and A. Spanias, "Bayesian optimization in high-dimensional spaces: A brief survey," in *2021 12th International conference on information, intelligence, systems & applications (IISA)*. IEEE, 2021.
- [27] A. A. Paranjape, S.-J. Chung, and J. Kim, "Novel dihedral-based control of flapping-wing aircraft with application to perching," *IEEE Transactions on Robotics*, 2013.
- [28] M. Zhou, M. Cui, D. Xu, S. Zhu, Z. Zhao, and A. Abusorrah, "Evolutionary optimization methods for high-dimensional expensive problems: A survey," *IEEE/CAA Journal of Automatica Sinica*, 2024.
- [29] S. Nadarajah and A. Jameson, "A comparison of the continuous and discrete adjoint approach to automatic aerodynamic optimization," in *38th Aerospace sciences meeting and exhibit*, 2000.
- [30] M. Dreha, "Xfoil: An analysis and design system for low reynolds number airfoils," in *Low Reynolds number aerodynamics: proceedings of the conference notre dame, Indiana, USA, 5-7 June 1989*. Springer, 1989.
- [31] J. C. Mason and D. C. Handscomb, *Chebyshev polynomials*. Chapman and Hall/CRC, 2002.
- [32] L. Brutman, "On the lebesgue function for polynomial interpolation," *SIAM Journal on Numerical Analysis*, 1978.
- [33] M. R. Hestenes, "Multiplier and gradient methods," *Journal of optimization theory and applications*, 1969.
- [34] D. M. Buede and W. D. Miller, *The engineering design of systems: models and methods*. John Wiley & Sons, 2024.
- [35] F.-M. De Rainville, F.-A. Fortin, M.-A. Gardner, M. Parizeau, and C. Gagné, "Deap: A python framework for evolutionary algorithms," in *Proceedings of the 14th annual conference companion on Genetic and evolutionary computation*, 2012.
- [36] B. M. Kulfan, "Universal parametric geometry representation method," *Journal of aircraft*, 2008.
- [37] A. Wächter and L. T. Biegler, "On the implementation of an interior-point filter line-search algorithm for large-scale nonlinear programming," *Mathematical programming*, 2006.